Available online at www.sciencedirect.com
SCIENCE DIRECT®
Journal of Solid State Chemistry 179 (2006) 81–90
JOURNAL OF SOLID STATE CHEMISTRY
www.elsevier.com/locate/jssc

Magnetic structures of the α-$Li_3Fe_2(PO_4)_{3-x}(AsO_4)_x$ ($x = 1$, 1.5, 2, 3) solid solution

Aintzane Goñi[a], José Luis Mesa[a], José Luis Pizarro[b], Leopold Fournés[c], Alain Wattiaux[c], Roger Olazcuaga[c], María Isabel Arriortua[b], Teófilo Rojo[a,*]

[a]*Dpto. Química Inorgánica, Facultad de Ciencia y Tecnología, UPV/EHU, Apdo. 644, E-48080 Bilbao, Spain*
[b]*Dpto. de Mineralogía y Petrología, Facultad de Ciencia y Tecnología, UPV/EHU, Apdo. 644, E-48080 Bilbao, Spain*
[c]*Institut de Chimie de la Matière Condensée de Bordeaux (ICMCB-CNRS), 33608 Pessac Cedex, France*

Received 26 July 2005; received in revised form 28 September 2005; accepted 28 September 2005
Available online 11 November 2005

Abstract

Mössbauer spectroscopy and neutron diffraction studies have been carried out for the α-$Li_3Fe_2(PO_4)_{3-x}(AsO_4)_x$ ($x = 1$, 1.5, 2, 3) solid solution, potential candidate for the cathode material of the lithium secondary batteries. The crystal and magnetic structures of all these phases are based on the structural and magnetic model corresponding to the α-$Li_3Fe_2(PO_4)_3$ phosphate parent, but with some differences promoted by the arsenate substitution. The PO_4 and AsO_4 groups have a random distribution in the structure. In all compounds the coupling of the magnetic moments takes place in the (001) plane, but the value of the angle between the moments and the x direction decreases from 38.3° (α-$Li_3Fe_2(AsO_4)_3$) to 4.7° (α-$Li_3Fe_2(PO_4)_2(AsO_4)_1$). This rotation arises from the change in the tilt angle between the $Fe(1)O_6$ and $Fe(2)O_6$ crystallographically and magnetically independent octahedra in the structures, and affects the effectiveness of the magnetic exchange pathways. The ordering temperature T_N decreases with the increase of phosphate amount in the compounds. The existence of a phenomenon of canting and the evolution of the ferrimagnetic behavior in this solid solution is also discussed.

Keywords: Iron (III) phosphate–arsenate; Crystal structure; Magnetic structure; Mössbauer spectroscopy; Magnetic properties

1. Introduction

In the new lithium battery technology, recent efforts have been devoted to the study of iron phosphates as materials for the cathode. Much interest centers on the olivine-type $LiFePO_4$ compound [1–4], but also on the Nasicon-related $Li_3Fe_2(PO_4)_3$ polymorphs [5,6] because of their favorable redox properties, good ionic conductivity and low cost. The interest of the different $Li_3Fe_2(PO_4)_3$ phases and their related arsenate compounds [7] lies in determining the factors that impact on the electrochemical behavior of the materials [8–11]. Detailed structural and magnetic studies of the rhombohedral and monoclinic forms of $Li_3Fe_2(PO_4)_3$ were recently reported by different authors [12–16]. As a part of our investigation works, the crystal structure of monoclinic α-$Li_3Fe_2(AsO_4)_3$ together with the spectroscopic and magnetic study on the isostructural α-$Li_3Fe_2(PO_4)_{3-x}(AsO_4)_x$ ($x = 1$, 1.5, 2, 3) solid solution were also published [17,18].

The structure of α-$Li_3Fe_2(XO_4)_3$ ($X = P$, As) was described as a three-dimensional framework of vertex-sharing FeO_6 octahedra and XO_4 tetrahedra. Each FeO_6 octahedron is surrounded by six XO_4 tetrahedra and each tetrahedron is linked to four FeO_6 polyhedra, making up the $[Fe_2(XO_4)_3]^{3-}$ open framework [19]. The lithium ions are distributed in three different crystal sites in the structure, filling the voids inside the iron phosphate or arsenate structure and compensating the negative charge (Fig. 1). There are two independent iron positions in the structure of these compounds, Fe(1) and Fe(2), which lead to the existence of two different magnetic sublattices [20]. The magnetic properties indicated the predominance of antiferromagnetic interactions between these sublattices, with the presence of a ferromagnetic component be1ow the ordering temperature (L-type ferrimagnetism). For every

*Corresponding author. Fax: +34 94 601 35 00.
E-mail addresses: teo.rojo@ehu.es, qiproapt@lg.ehu.es (T. Rojo).

0022-4596/$ - see front matter © 2005 Elsevier Inc. All rights reserved.
doi:10.1016/j.jssc.2005.09.048

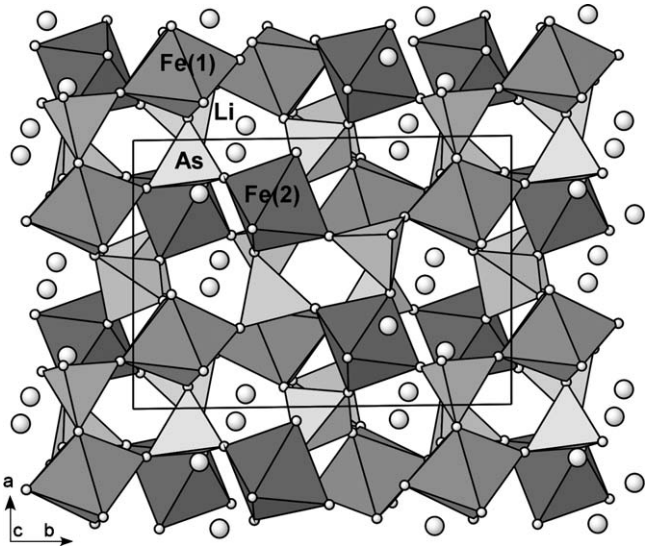

Fig. 1. Polyhedral representation of the α-$Li_3Fe_2(AsO_4)_3$ crystal structure view along the [001] direction.

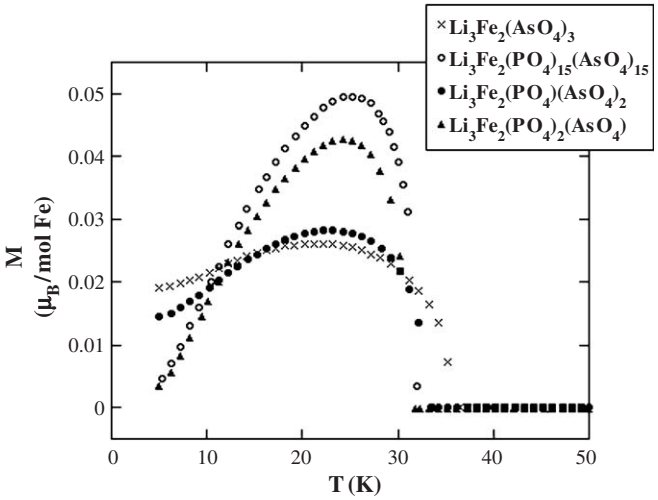

Fig. 2. Field-cooled magnetization measurements at 0.1 T of $Li_3Fe_2(PO_4)_{3-x}(AsO_4)_x$ ($x = 1$, 1.5, 2, 3).

phase, the field-cooled magnetization exhibits a rapid increase of its value just below T_N (Fig. 2) reaching a maximum, and tending to different magnetization values when T tends towards zero.

Neutron diffraction and Mössbauer studies of α-$Li_3Fe_2(PO_4)_3$ showed the existence of weak ferrimagnetism in this compound. However, in the case of $Li_3Fe_2(PO_4)_{3-x}(AsO_4)_x$ ($x = 1$, 1.5, 2, 3) another phenomenon has been also detected. The remanent magnetization does not tend towards zero at 0 K, as could be expected if only ferrimagnetic behavior was present. So, a slight canting of the magnetic moments of the Fe(l) and Fe(2) sublattices in the ordered state has been considered. The canting angle should decrease with decreasing the amount of arsenate in the compounds, becoming practically negligible for the $Li_3Fe_2(PO_4)_3$ phase. In this sense, it should be interesting to determine the evolution of the magnetic structure with the arsenate content in $Li_3Fe_2(PO_4)_{3-x}(AsO_4)_x$. Hence, in this paper we describe the neutron diffraction and Mössbauer spectroscopy studies on the α-$Li_3Fe_2(PO_4)_{3-x}(AsO_4)_x$ ($x = 1$, 1.5, 2, 3) solid solution, which have been undertaken in order to elucidate the crystallographic and magnetic structures of $Li_3Fe_2(PO_4)_{3-x}(AsO_4)_x$ and also to explain the magnetic behavior in this solid solution.

2. Experimental

Neutron powder diffraction measurements were performed on the D1B and D2B powder diffractometers, at the Institute Laue-Langevin of Grenoble, using wavelengths of 2.52 and 1.595 Å, respectively. About 5.0 g of each sample, contained in a cylindrical vanadium can and held in a liquid-helium cryostat, were employed in the experiments. The high resolution of D2B was used to obtain extensive and accurate structural data of $Li_3Fe_2(PO_4)_{1.5}(AsO_4)_{1.5}$ and $Li_3Fe_2(AsO_4)_3$ at room temperature, over a large angular range $10^\circ \leqslant 2\theta \leqslant 160^\circ$. The high flux and medium resolution of D1B were used to study the thermal evolution of the $Li_3Fe_2(PO_4)_{3-x}(AsO_4)_x$ ($x = 1$, 1.5, 2, 3) samples, in the temperature range 1.5–100 K. The diffraction patterns were collected every 2 K for 300 s in the angular range $10^\circ \leqslant 2\theta \leqslant 90^\circ$. The Rietveld program FULLPROF [21] was used to refine the crystal and magnetic structures. The backgrounds were fitted to a polynomial function. The thermal dependent D1B diffraction data were refined sequentially, taking as starting parameters of each pattern those resulting from the final refinement of the precedent one. A pseudo-Voigt function was chosen to generate the line shape of the diffraction peaks.

Mössbauer spectroscopy measurements were performed. The spectra of $Li_3Fe_2(PO_4)_{3-x}(AsO_4)_x$ ($x = 1$, 1.5, 2, 3) were recorded at 4.2 and 293 K. Moreover, for $x = 1.5$ and 3, a thermal study of the Mössbauer signals was carried out between 4.2 and 32 K. The measurements were performed with a constant acceleration Halder-type spectrometer using a ^{57}Co source in a Rh matrix. The velocity was calibrated with pure iron metal as a standard material. All isomer shifts reported in this work refer to the natural α–Fe at 293 K. Low-temperature spectra were recorded using a liquid-helium flow cryostat.

3. Results

3.1. Room temperature structures

The room-temperature D2B powder neutron diffraction patterns of $Li_3Fe_2(AsO_4)_3$ and $Li_3Fe_2(PO_4)_{1.5}(AsO_4)_{1.5}$ were refined using the Rietveld method taking as starting model the $Li_3Fe_2(PO_4)_3$ crystal structure reported in Ref. [19]. For the $Li_3Fe_2(PO_4)_{1.5}(AsO_4)_{1.5}$ compound the best fit of the powder diffraction data was obtained with a structural model in which the P and As ions have a

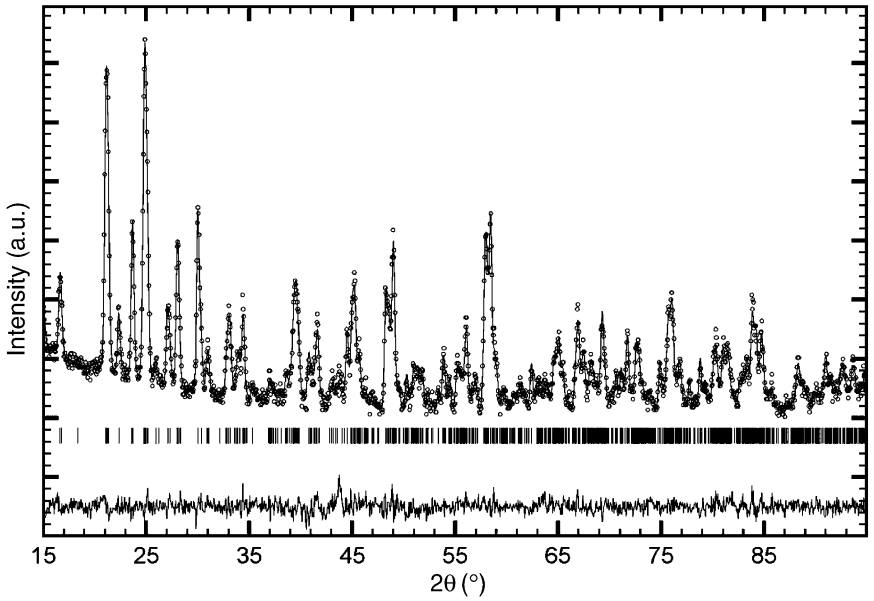

Fig. 3. Observed (circles), calculated (solid line) and difference (at the bottom with the same scale) neutron diffraction profiles (D2B, ILL) of $Li_3Fe_2(PO_4)_{1.5}(AsO_4)_{1.5}$ at room temperature. Vertical marks correspond to the position of the Bragg reflections.

Table 1
Crystal structure parameters and reliability factors for D2B data Rietveld refinements of $Li_3Fe_2(PO_4)_{3-x}(AsO_4)_x$ ($x = 3$, 1.5)

	$Li_3Fe_2(AsO_4)_3$	$Li_3Fe_2(PO_4)_{1.5}(AsO_4)_{1.5}$
a (Å)	8.6049(1)	8.6614(5)
b(Å)	12.2111(1)	12.1784(7)
c(Å)	8.9252(1)	8.7294(5)
γ (deg)	90.758(1)	90.705(4)
V (Å^3)	937.74(2)	920.73(9)
Rp (%)	4.08	3.38
R_{wp} (%)	5.12	4.46
R_{expt} (%)	3.55	3.46
χ^2	2.08	1.54
R_B (%)	4.58	6.54

Space group $P1121/n$ (No. 14), $Z = 4$, $T = 293$ K.

random distribution into three independent tetrahedral positions. The experimental, ca1culated and difference neutron powder diffraction profiles for $Li_3Fe_2(PO_4)_{1.5}(AsO_4)_{1.5}$ are shown in Fig. 3. The room temperature structural parameters and the reliability factors from D2B data refinements are summarized in Table 1. Atomic coordinates and thermal parameters for $Li_3Fe_2(AsO_4)_3$ and $Li_3Fe_2(PO_4)_{1.5}(AsO_4)_{1.5}$ compounds are given as supplementary material. Table 2 shows the interatomic distances and angles.

Two significant differences have been observed between the structures of both compounds. The first one is the evolution of the X–O distances inside the XO_4 (X = P, As) tetrahedra as a result of the arsenate-phosphate substitution. The values of the mean X–O bond lengths are 1.68(1) and 1.60(2) Å, for $Li_3Fe_2(AsO_4)_3$ and $Li_3Fe_2(PO_4)_{1.5}(AsO_4)_{1.5}$, respectively, showing the expected reduction of the bond distances from the arsenate to the phosphate groups. This fact does not cause any relevant evolution in the Fe–O distances inside the FeO_6 octahedra.

The second difference involves the relative orientation of the two independent FeO_6 octahedra in the unit cells of $Li_3Fe_2(AsO_4)_3$ and $Li_3Fe_2(PO_4)_{1.5}(AsO_4)_{1.5}$ (Fig. 4). As can be observed, the Fe(1)O_6 octahedra maintain, approximately, their orientation in both compounds whereas the Fe(2)O_6 octahedra modify their tilt angle with respect to the x-axis in appreciable form. The change in the orientation of the octahedra can be quantified by measuring the angles between [100], [010] and [001] directions and the major axis of each FeO_6 octahedron, O(3)–Fe(1)–O(6) for Fe(1)O_6 and O(5)–Fe(2)–O(4) for Fe(2)O_6. From $Li_3Fe_2(AsO_4)_3$ to $Li_3Fe_2(PO_4)_{1.5}(AsO_4)_{1.5}$, the tilt of the Fe(1)$O_6$ polyhedron changes in $-1.62°$ (with respect to the x-axis), $+1.15°$ (with respect to the y-axis) and $+1.31°$ (with respect to the z-axis). However, the orientation of the Fe(2)O_6 octahedron is modified in $-13.74°$ (with respect to the x-axis), $-6.67°$ (with respect to the y-axis) and $+2.92°$ (with respect to the z-axis). In this sense, for $Li_3Fe_2(PO_4)_3$ the Fe(1)O_6 and Fe(2)O_6 polyhedra are related by a pseudo-glide plane (pseudo-symmetry operation $[1/2 + x, 1/2 - y, z]$) [19], but the pseudo-symmetry is gradually lost when decreasing the amount of phosphate.

3.2. Mössbauer spectroscopy

The Mössbauer spectra of $Li_3Fe_2(PO_4)_{3-x}(AsO_4)_x$ ($x = 1$, 1.5, 2, 3) recorded at 293 and 4.2 K are similar. The spectrum of $Li_3Fe_2(PO_4)_{1.5}(AsO_4)_{1.5}$ is shown in Fig. 5 as representative. The spectra in the paramagnetic state are typical of high-spin Fe^{3+} ions in slightly distorted

Table 2
Bond distances (bold) (Å) and angles (deg) for room temperature D2B data Rietveld refinements of $Li_3Fe_2(PO_4)_{3-x}(AsO_4)_x$ ($x = 3$, 1.5).

			$Li_3Fe_2(AsO_4)_3$			
[Fe(1)O_6]						
Fe(1)	O(1)^{i}	O(3)	O(6)^{ii}	O(7)	O(9)^{i}	O(11)
O(11)	85.4(2)	79.6(2)	92.3(3)	96.0(3)	164.6(3)	**2.029(6)**
O(9)^{I}	82.4(2)	90.2(2)	99.1(3)	93.5(3)	**1.994(6)**	
O(7)	165.8(3)	79.9(2)	94.4(3)	**2.000(6)**		
O(6)^{ii}	99.7(3)	169.5(3)	**1.869(6)**			
O(3)	86.5(2)	**2.054(6)**				
O(1)^{I}	**2.059(6)**					
[Fe(2)O_6]						
Fe(2)	O(2)^{iii}	O(4)	O(5)	O(8)	O(10)^{iii}	O(12)
O(12)	94.2(3)	79.7(2)	106.3(3)	87.6(2)	160.5(3)	**1.989(6)**
O(10)^{iii}	95.8(2)	83.5(2)	90.3(2)	83.2(2)	**1.961(6)**	
O(8)	177.1(2)	91.9(2)	86.1(2)	**2.088(6)**		
O(5)^{iv}	91.1(2)	173.6(3)	**1.990(5)**			
O(4)	90.7(2)	**2.106(5)**				
O(2)^{iii}	**1.967(6)**					
[As(1)O_4]						
As(1)	O(2)^{v}	O(3)^{vi}	O(5)	O(11)		
O(11)	116.3(4)	108.1(3)	107.7(3)	**1.682(7)**		
O(5)	113.3(3)	100.7(3)	**1.715(6)**			
O(3)^{vi}	109.5(5)	**1.659(7)**				
O(2)^{v}	**1.695(7)**					
[As(2)O_4]						
As(2)	O(1)^{v}	O(4)^{vii}	O(6)	O(12)		
O(12)	101.5(3)	116.8(4)	106.8(4)	**1.695(7)**		
O(6)	109.4(3)	112.7(3)	**1.676(7)**			
O(4)^{vii}	108.9(4)	**1.671(7)**				
O(1)^{v}	**1.712(7)**					
[As(3)O_4]						
As(3)	O(7)^{vii}	O(8)^{v}	O(9)	O(10)^{viii}		
O(10)^{viii}	100.3(3)	112.7(4)	107.9(4)	**1.701(7)**		
O(9)	110.0(4)	107.7(3)	**1.669(7)**			
O(8)^{v}	117.7(4)	**1.669(7)**				
O(7)^{vii}	**1.663(7)**					
			$Li_3Fe_2(PO4)_{1.5}(AsO_4)_{1.5}$			
[Fe(1)O_6]						
Fe(1)	O(1)^{i}	O(3)	O(6)^{ii}	O(7)	O(9)^{i}	O(11)
O(11)	89.3(6)	78.7(6)	88.8(6)	95.4(6)	167.6(7)	**2.04(1)**
O(9)^{i}	81.5(6)	92.0(6)	100.6(6)	91.7(7)	**1.99(1)**	
O(7)	165.9(7)	83.5(6)	95.8(7)	**1.94(1)**		
O(6)^{ii}	97.6(7)	167.4(7)	**1.89(1)**			
O(3)	84.3(6)	**2.06(1)**				
O(1)^{i}	**2.03(2)**					
[Fe(2)O_6]						
Fe(2)	O(2)^{iii}	O(4)	O(5)	O(8)	O(10)^{iii}	O(12)
O(12)	89.3(6)	74.3(6)	97.1(7)	84.7(6)	163.0(7)	**2.04(2)**
O(10)^{iii}	94.1(6)	89.7(5)	99.6(7)	89.2(6)	**1.88(1)**	
O(8)	169.3(6)	89.3(6)	99.1(7)	**1.99(1)**		
O(5)^{iv}	90.5(7)	167.5(7)	**1.91(2)**			
O(4)	80.5(5)	**2.19(1)**				
O(2)^{iii}	**2.04(1)**					

Table 2 (*continued*)

$Li_3Fe_2(PO4)_{1.5}(AsO_4)_{1.5}$						
$[Fe(1)O_6]$						
Fe(1)	O(1)^{i}	O(3)	O(6)^{ii}	O(7)	O(9)^{i}	O(11)
$[As/P(1)O_4]$						
As/P(1)	O(2)^{v}	O(3)^{vi}	O(5)	O(11)		
O(11)	106.3(9)	109.1(9)	110.7(10)	**1.64(2)**		
O(5)	115.8(10)	107.7(10)	**1.55(2)**			
O(3)^{vi}	107.1(9)	**1.59(2)**				
O(2)^{v}	**1.60(2)**					
[As/P(2)O4]						
As/P(2)	O(1)^{v}	O(4)^{vii}	O(6)	O(12)		
O(12)	104.6(9)	114.3(9)	107.1(9)	**1.67(2)**		
O(6)	113.0(10)	108.2(9)	**1.59(2)**			
O(4)^{vii}	109.7(9)	**1.61(2)**				
O(1)v	**1.59(2)**					
[As/P(3)O4]						
As(3)	O(7)^{viii}	O(8)^{v}	O(9)	O(10)^{viii}		
O(10)^{viii}	102.2(10)	112.1(10)	108.0(9)	**1.63(2)**		
O(9)	112.5(10)	111.7(9)	**1.55(2)**			
O(8)^{v}	108.0(9)	**1.56(2)**				
O(7)^{viii}	**1.63(2)**					

(i) $(1/2-x, 1/2-y, 1/2-z)$; (ii) $(-1/2+x, -1/2+y, 1/2-z)$; (iii) $(3/2-x, 1/2-y, 1/2+z)$; (iv) $(1/2+x, 1/2+y, 1/2-z)$; (v) $(-1+x, y, z)$; (vi) $(-1/2+x, 1/2-y, -1/2+z)$; (vii) $(-3/2-x, 1/2-y, -1/2+z)$; (vii) $(-1/2+x, 1/2+y, 1/2-z)$.

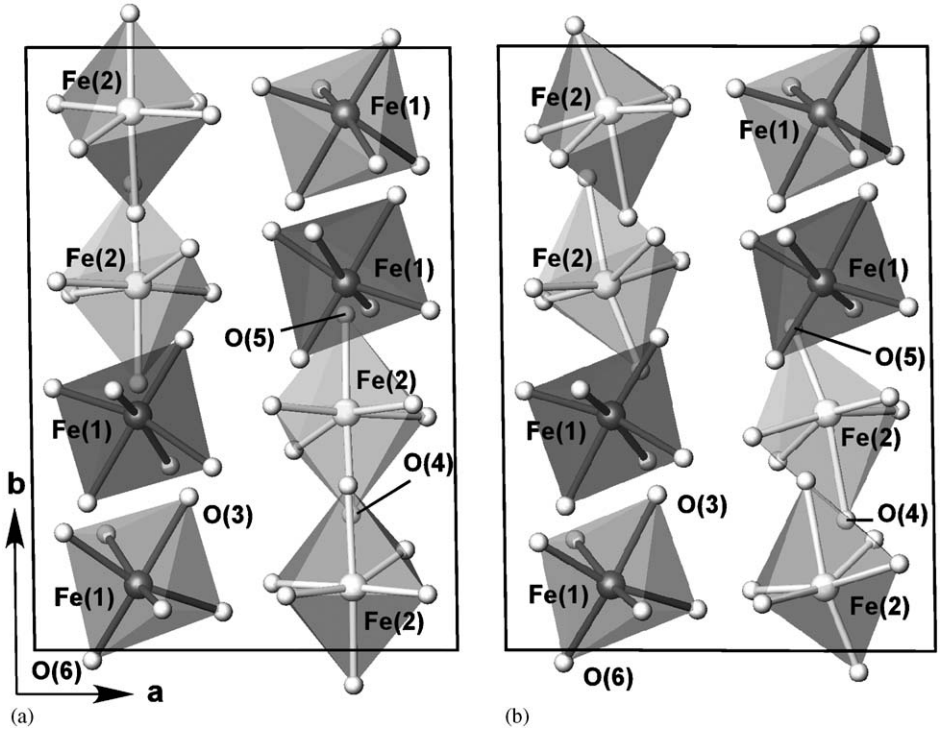

Fig. 4. Relative orientation of both $Fe(1)O_6$ and $Fe(2)O_6$ octahedra for (a) $Li_3Fe_2(AsO_4)_3$ and (b) $Li_3Fe_2(PO_4)_{1.5}(AsO_4)_{1.5}$, showing the different tilt angle on the $Fe(2)O_6$ polyhedra.

octahedral environment. These spectra were satisfactorily fitted with a single doublet in each case, in spite of the existence of two different Fe sites in the structures. This fact is probably due to the existence in theses phases of very similar Fe–O bond distances. Furthermore, the disorder in the crystal structure of the $(PO_4)^{3-}$ and $(AsO_4)^{3-}$

oxoanions originates the existence of only one environment for the two FeO_6 octahedra and, therefore, only one site with a distribution of quadrupolar splittings is observed in the Mössbauer spectra. The fitting parameters are summarized in Table 3.

The spectra at 4.2 K for every composition can be described as a single magnetic sextet, representative of magnetically ordered Fe^{3+} ions octahedrically coordinated. The calculated values of magnetic hyperfine fields B near to 55 T (Table 2) are in good agreement with the presence of Fe^{3+} in high spin configuration. Some differences can be observed in the chemical shifts δ of every phase at 293 and 4.2 K, which correspond to the second-order Doppler effect.

The increase of the arsenate content x in the samples leads to lower values of δ and B. This fact can be attributed to the smaller volume of PO_4 than AsO_4. Taking into account the principle of the antagonic bonds, the lengthening of the X–O bond distance with the increase of arsenate induces a small increase of covalence in the Fe–O bonds, reducing the chemical shift. The existence of disorder between the PO_4 and AsO_4 groups around the Fe^{3+} ions can be deduced from the distribution diagrams of the quadrupole shifts for each composition. This disorder becomes clearer for the intermediate phases in which the phosphate and arsenate contents are similar.

A study of the thermal evolution of the Mössbauer spectra has been carried out in the $4.2\,K < T < 32\,K$ temperature range, for the $Li_3Fe_2(AsO_4)_3$ and $Li_3Fe_2(PO_4)_{1.5}(AsO_4)_{1.5}$ compounds. T_N values of 31(1) and 27(1) K have been obtained, by the analysis of the temperature dependence of the hyperfine fields (see Fig. 6), for the arsenate pure phase and mixed phosphate–arsenate phase, respectively. In both compounds, the magnetic transition is sharp with only a narrow temperature region of coexisting magnetic and non-magnetic components.

All the low-temperature spectra for $Li_3Fe_2(AsO_4)_3$ can be well fitted with a single magnetic sextet. However, for $Li_3Fe_2(PO_4)_{1.5}(AsO_4)_{1.5}$, unusual broadnesses of the lines (values around 1 mm s^{-1} for the Γ parameter) have been obtained from transition temperature to 18 K. This widening can be explained by the existence of overlapped signals corresponding to two different magnetic sextets from two magnetic sublattices, with almost equal chemical and quadrupole shifts, but slightly different internal hyperfine fields. This behavior was also observed for the $Li_3Fe_2(PO_4)_3$ phase [20] (see the inset in Fig. 6), which was atributted to the existence of weak ferrimagnetism originated from the existence of two crystallographically different Fe^{3+} sites in the compound.

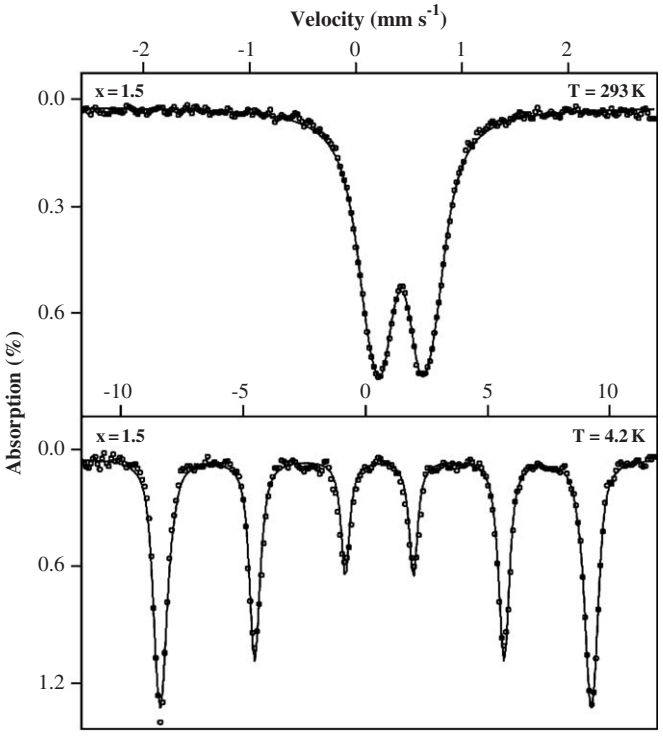

Fig. 5. Observed (circles) and calculated (line) Mössbauer spectrum of $Li_3Fe_2(PO_4)_{1.5}(AsO_4)_{1.5}$ at 293 and 4.2 K temperatures.

3.3. Low-temperature neutron diffraction and magnetic structure refinement

The D1B neutron diffraction patterns recorded at low temperatures for all $Li_3Fe_2(PO_4)_{3-x}(AsO_4)_x$ ($x = 1$, 1.5, 2, 3) compounds are very similar. Fig. 7 shows the thermal evolution of the diffraction patterns from 100 to 1.5 K for $Li_3Fe_2(PO_4)_{1.5}(AsO_4)_{1.5}$. The extra peak at $d = 6.9$ Å, clearly observed at 1.5 K, corresponds to the purely magnetic part of the scattering. This intense magnetic reflection can be indexed as a superposition of the (110)

Table 3
Mössbauer parameters of $Li_3Fe_2(PO_4)_{3-x}(AsO_4)_x$ ($x = 1$, 1.5, 2, 3) at 293 and 4.2 K

	$T = 293$ K			$T = 4.2$ K		
x	δ (mm s^{-1})	Γ (mm s^{-1})	Δ (mm s^{-1})	δ (mm s^{-1})	ε (mm s^{-1})	B (T)
1	0.444	0.30	0.456	0.556	−0.0762	55.30
1.5	0.437	0.30	0.469	0.546	−0.0738	54.94
2	0.438	0.30	0.482	0.539	−0.0101	54.86
3	0.395	0.25	0.464	0.534	−0.0918	54.67

and (011) Bragg reflections, which have negligible structure factors in the nuclear structure. Moreover, the intensities at 1.5 K of some nuclear peaks increase due to the magnetic contribution. All magnetic peaks have been indexed using the propagation vector $k = (000)$, which indicates that the magnetic unit cell is the same as the nuclear one.

The magnetic structure refinements were performed using the FULLPROF program [21], in which the crystal and magnetic structures are considered as a coupled two-phase system. When available ($x = 1.5$, 3), the starting structural model was that obtained at room temperature. For $x = 2$ and 1, the starting parameters were deduced from the atomic coordinates of $x = 1.5$, correcting the occupation factors for the randomly distributed P and As atoms. The magnetic structure was included in the refinements as an independent phase for which only magnetic atoms were defined and only magnetic scattering was calculated. The scale and thermal factors were constrained for both nuclear and magnetic structures. Moreover, the magnetic moments of the Fe(1) and Fe(2) atoms were constrained to be equal.

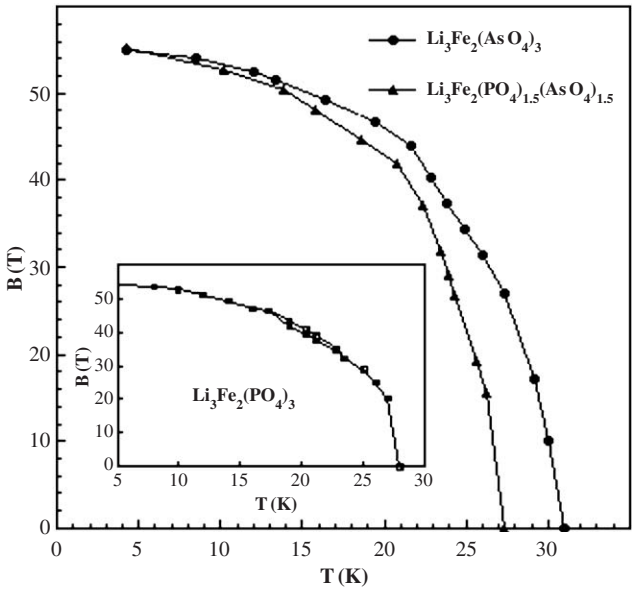

Fig. 6. Temperature dependence of the hyperfine fields for the observed Mössbauer spectra of $Li_3Fe_2(PO_4)_{3-x}(AsO_4)_x$ ($x = 1.5$, 3). The curve corresponding to $Li_3Fe_2(PO_4)_3$ has been included in the inset for comparison.

The magnetic structures compatible with the crystal symmetry were evaluated with the help of group-theory calculations. Taking into account the space group $P112_1/n$ of these compounds, the possible arrangements of the magnetic moments were considered. As was previously indicated, the magnetic ions in the unit cell occupy two different 4(*e*) general sites in the crystal structure: Fe(1) (named *R*), is placed at about (0.25, 0.1, 0.5), and Fe(2) (named *S*) at about (0.75, 0.4, 0.5). It is to note that these two positions are related by the $(1/2+x, 1/2-y, z)$ pseudo-symmetry element (glide plane *a* perpendicular to the *y*-axis), present in the orthorhombic high-temperature phase of the $Li_3Fe_2(PO_4)_3$ compound (space group *Pcan*) [19]. The location of the 8 iron atoms in the unit cell is deduced from the *R* and *S* sites by the symmetry operators: (1) (x, y, z); (2) 2_{1z} $(1/2-x, 1/2-y, 1/2+z)$; (3) n_z $(1/2+x, 1/2+y, 1/2-z)$ and (4) i $(-x, -y, -z)$. The different possibilities of magnetic configurations were investigated using Bertaut's symmetry analysis method [22,23] that allows determining the symmetry constraints between magnetic moments of atoms belonging to whatever crystallographic site. The four possible couplings of the magnetic moments inside *R* and *S* sublattices are *F* (+ + + +), *G* (+ − + −),

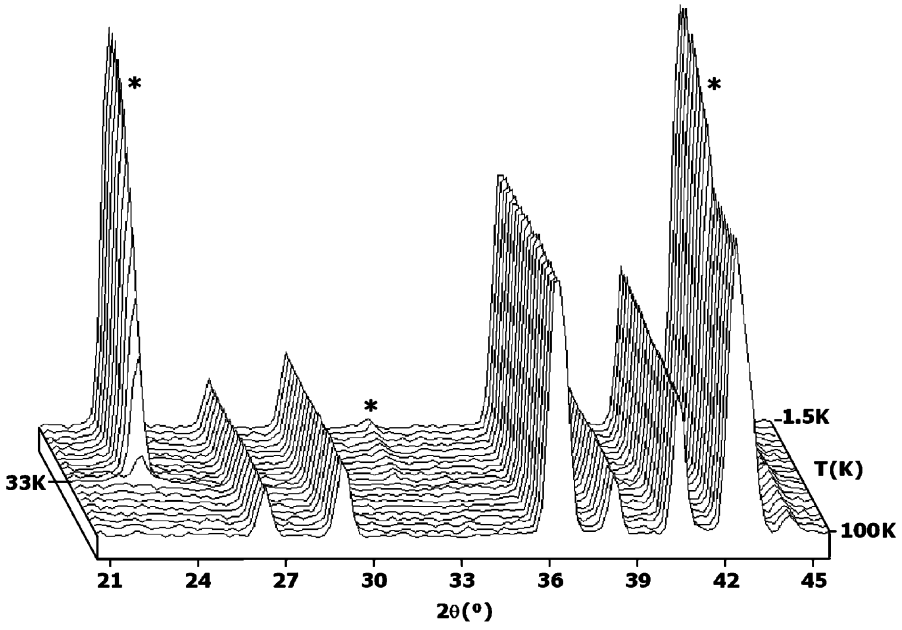

Fig. 7. Thermal evolution of the D1B neutron diffraction patterns of $Li_3Fe_2(AsO_4)_{1.5}(PO_4)_{1.5}$.

C $(++--)$ and A $(+--+)$. The irreducible representations corresponding to the possible magnetic structures (space group $P112_1/n$) of the R or S sublattices are described in Table 4.

Table 4
Irreducible representations corresponding to the possible magnetic structures of the R or S sublattices (space group $P1121/n$)

	R or S sublattice		
	x	y	z
Γ_1	A_x	A_y	F_z
Γ_2	G_x	G_y	C_z
Γ_3	C_x	C_y	G_z
Γ_4	F_z	F_y	A_z

Table 5
Refined magnetic moments of iron ions and the Rietveld reliability factor for $Li_3Fe_2(PO_4)_{3-x}(AsO_4)_x$ ($x = 1, 1.5, 2, 3$)

x	3	2	1.5	1
M_x (μ_B)	3.68(8)	4.0(1)	4.52(4)	4.51(3)
M_y (μ_B)	2.8(1)	2.2(2)	0.7(2)	0.4(2)
M_z (μ_B)	4.56(3)	4.49(3)	4.56(3)	4.52(3)
Φ (deg)	38.3	28.7	9.0	4.7
R_p (%)	1.72	2.13	1.9	1.75
R_{wp} (%)	2.33	2.87	2.45	2.35
χ^2	8.77	13.10	9.40	9.28
R_{nucl} (%)	2.80	3.74	4.73	3.23
R_{mag} (%)	5.28	3.38	3.92	3.29

Φ is the angle formed by the magnetic moments with x direction.
M_x (μ_B) = 5.0(2), M_y (μ_B) = 0, M_z (μ_B) = 5.0(2) and Φ (deg) = 0. Data for $Li_3Fe_2(PO_4)_3$ ($x = 0$) obtained from Ref. [16].

As pointed out in previous works [17], the magnetic behavior of the $Li_3Fe_2(PO_4)_{3-x}(AsO_4)_x$ ($x = 1, 1.5, 2, 3$) phases was described as ferrimagnetic due to the incomplete compensation of the antiparallel magnetic moments resulting from the two different ferromagnetic sublattices. So, taking into account the possible arrangements of the magnetic moments showed in Table 5, only the Γ_1 and Γ_4 representations agree with a ferromagnetic coupling in each sublattice. For the Γ_1 representation the magnetic interactions are ferromagnetic in the [001] direction, while in Γ_4 the moments are ferromagnetically coupled in the (001) plane. The global antiferromagnetic behavior (R–S) can be obtained reversing the relative moment orientation of the sublattices by $\Gamma(R)_1-\Gamma(S)_1$ or by $\Gamma(R)_4-\Gamma(S)_4$. In the $\Gamma(R)_1-\Gamma(S)_1$ model the relationships between the 8 moments in the unit magnetic cell are $[R(1)-R(2)-R(3)+R(4)-S(1)+S(2)+S(3)-S(4)]_x$, $[R(1)-R(2)-R(3)+R(4)-S(1)+S(2)+S(3)-S(4)]_y$ and $[R(1)+R(2)+R(3)+R(4)-S(1)-S(2)-S(3)-S(4)]_z$. In the $\Gamma(R)_4-\Gamma(S)_4$ model the relationships are $[R(1)+R(2)+R(3)+R(4)-S(1)-S(2)-S(3)-S(4)]_x$, $[R(1)+R(2)+R(3)+R(4)-S(1)-S(2)-S(3)-S(4)]_y$ and $[R(1)-R(2)-R(3)+R(4)-S(1)+S(2)+S(3)-S(4)]_z$. We tried to fit both magnetic models by Rietveld method on the neutron diffraction data of $Li_3Fe_2(PO_4)_{3-x}(AsO_4)_x$ ($x = 1, 1.5, 2, 3$) recorded at 1.5 K, and the best agreement between observed and calculated patterns (see Fig. 8) was obtained for the $\Gamma(R)_4-\Gamma(S)_4$ model [Fe(1)–Fe(2) antiferromagnetic ordering in the (001) plane]. No significant magnetic component was observed along the z direction.

Table 5 summarizes the refined magnetic moments as well as the reliability factors obtained for all phases at

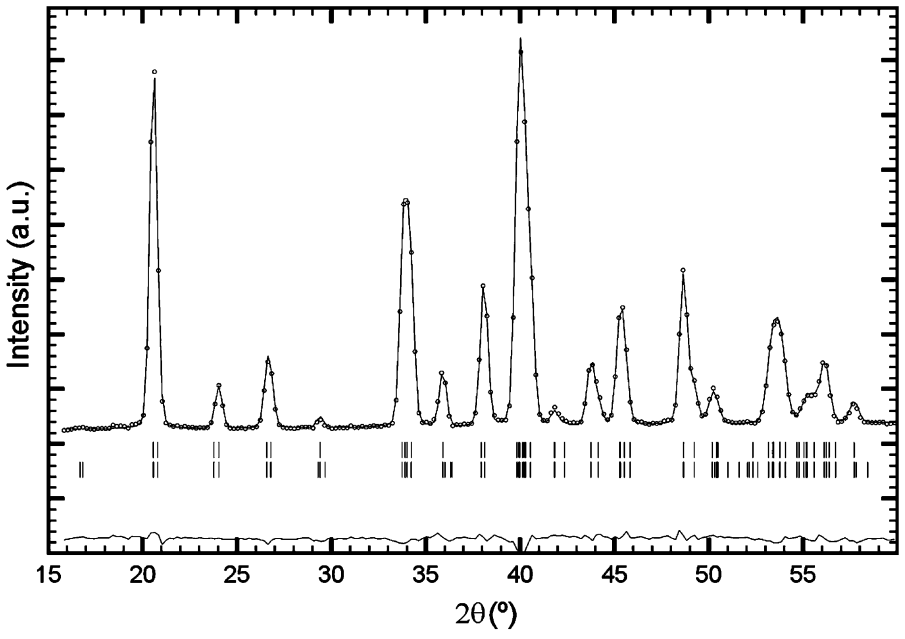

Fig. 8. Observed (circles), calculated (solid line) and difference (at the bottom with the same scale) neutron diffraction profiles (D1B, ILL) of $Li_3Fe_2(PO_4)_{1.5}(AsO_4)_{1.5}$ at 1.5 K. The first vertical marks correspond to the position of the nuclear reflections, and the second series represents the magnetic reflections.

1.5 K. The representation of the magnetic structure of $Li_3Fe_2(PO_4)_{1.5}(AsO_4)_{1.5}$ is shown in Fig. 9. In every case the four Fe atoms of R sublattice have magnetic moments parallel in the xy plane and the four moments of the S sublattice are antiparallel to the former.

The saturated magnetic moments of the Fe^{3+} ions are 4.56(3), 4.49(3), 4.56(3) and 4.52(3) μ_B per Fe^{3+} ion, for $x = 3$, 2, 1.5 and 1, respectively. The thermal evolution of the ordered magnetic moments for the studied phases shows that the ordering temperature T_N decreases with increasing the phosphate amount in the compounds, in good agreement with the results obtained from the magnetic measurements. The main difference in the magnetic structures of these compounds is the value of the Φ angle between the magnetic moments and x direction, which decreases from 38.3° ($x = 3$) to 4.7° ($x = 1$) (Fig. 10). The magnetic structure of $Li_3Fe_2(PO_4)_3$ [16] displayed the magnetic moments aligned along x direction ($\Phi = 0°$), in good agreement with the evolution of Φ observed in this work.

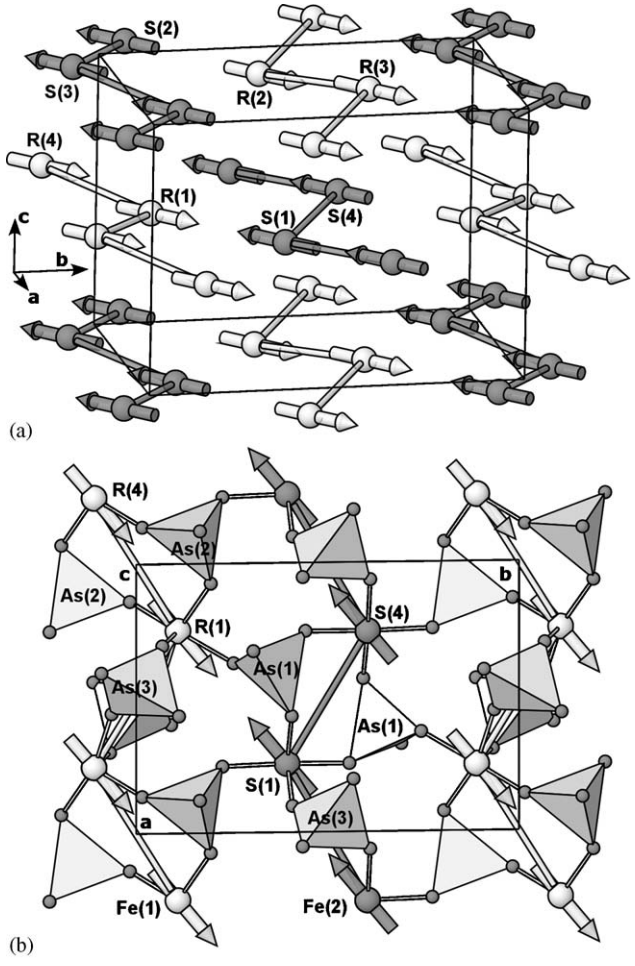

Fig. 9. (a) Three-dimensional representation of the Fe^{3+} moments on the magnetic structure of $Li_3Fe_2(PO_4)_{1.5}(AsO_4)_{1.5}$. (b) Projection on (001) showing the position of the bridge tetrahedra between irons. White and gray spheres represent the two types of crystallographic independent Fe^{3+} ions (R and S). The arrows indicate the direction of the magnetic moments.

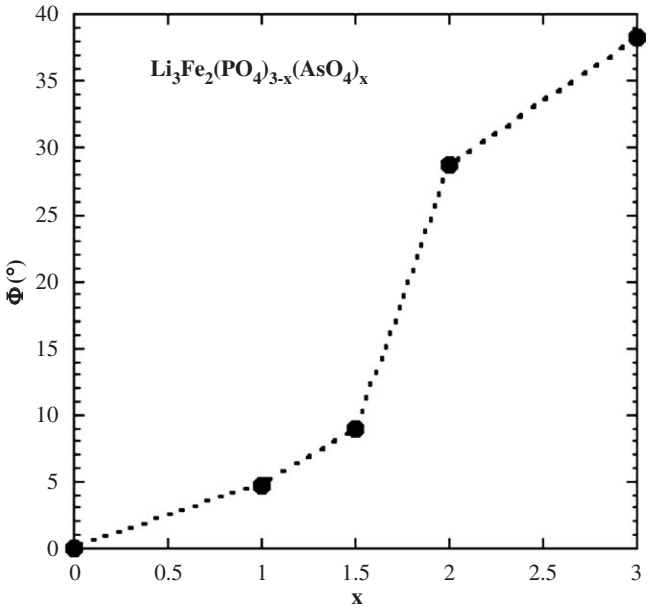

Fig. 10. Evolution of the Φ angle between the magnetic moments and the [100] direction in $Li_3Fe_2(PO_4)_{3-x}(AsO_4)_x$.

Finally, from the data recorded on D1B, we cannot estimate the spin canting assumed as origin of the remanent magnetization observed at lowest temperatures in the $Li_3Fe_2(PO_4)_{3-x}(AsO_4)_x$ solid solution. The slight misalignment of the magnetic moments corresponds to few tenths of degree, and so, it is difficult to establish a difference between them from the standard deviation in the values of the Φ angle.

4. Discussion and conclusions

The magnetic interactions in the substitutional solid solution $Li_3Fe_2(PO_4)_{3-x}(AsO_4)_x$ ($x = 1$, 1.5, 2, 3) are established through the AsO_4 and PO_4 groups involving Fe–O–(As, P)–O–Fe superexchange pathways. The phosphate and arsenate groups are distributed at random, disordered over the three independent tetrahedral sites. So, the interatomic distances and angles in the structure correspond to average values, which progressively develop with the replacement of arsenate by phosphate. This fact induces a progressive evolution of magnetic properties. The decrease of the magnetic ordering temperature observed from $Li_3Fe_2(AsO_4)_3$ to $Li_3Fe_2(PO_4)_3$, allow us to conc1ude that in this family of compounds the presence of AsO_4 groups increases the exchange interaction parameter, J, between the Fe atoms. However, this fact is difficult to explain considering the bond distances observed in the exchange pathways.

The evolution of the spin direction with the arsenate content is a more relevant factor. The coupling direction of the magnetic moments rotates an angle upper than 38° inside the xy plane, from $Li_3Fe_2(AsO_4)_3$ to $Li_3Fe_2(PO_4)_3$.

This rotation probably arises from the change in the tilt angle of the $Fe(2)O_6$ octahedra in the same plane of the crystal structure, affecting to the effectiveness of the magnetic exchange pathways.

The weak ferrimagnetism observed in the $Li_3Fe_2(PO_4)_{3-x}(AsO_4)_x$ solid solution is also affected by the arsenate–phosphate substitution. As was observed in the Mössbauer measurements, the increase of the arsenate percentage in the samples makes more difficult the resolution of the two magnetic sextets, which clearly appears for the $Li_3Fe_2(PO_4)_3$ compound. A unique magnetic sextet is observed for the magnetic ordered $Li_3Fe_2(AsO_4)_3$ phase in all temperature range. Considering that the magnetic model is the same for all compounds, i.e., two ferromagnetic sublattices antiferromagnetically coupled, this fact can be attributed to the strengthening of the antiferromagnetic interaction between Fe(1) and Fe(2) ferromagnetic sublattices in the arsenate $Li_3Fe_2(AsO_4)_3$ compound. For these structures the crystallographically inequivalent iron sites display different temperature dependences for the molecular field, giving rise to a phenomenon of *L*-type ferrimagnetism [24].

The two independent FeO_6 octahedra in the $Li_3Fe_2(PO_4)_3$ compound show planar pseudo-symmetry, avoiding the existence of canting between the coupled magnetic moments. Thus pseudo-symmetry between $Fe(1)O_6$ and $Fe(2)O_6$ disappears with the arsenate substitution, allowing the presence of weak ferromagnetism in the $Li_3Fe_2(PO_4)_{3-x}(AsO_4)_x$ ($x = 1$, 1.5, 2, 3) phases. The existence of canting becomes more evident as the arsenate content increases. However, taking into account the magnitude of the remanent magnetization value in every phase, the misalignment of the magnetic moments corresponds to a few tenths of degree, which is not detectable from the neutron diffraction data.

Acknowledgments

This work was financially supported by the Ministerio de Ciencia y Tecnología (BQU2001-0678) and the Universidad del País Vasco/Euskal Herriko Unibertsitatea (9/UPV 00130.310–13700/2001; 9/UPV 00130.310–15967/2004), which we gratefully acknowledge. We thank M.T. Fernández-Díaz from the Institute Laue-Langevin (ILL) Grenoble, France, for help in the neutron diffraction measurements carried out in the D1B and D2B powder diffractometers.

Appendix A. Supplementary materials

Supplementary data associated with this article can be found in the online version at doi:10.1016/j.jssc.2005.09.048

References

[1] C. Delacourt, P. Poizot, J.M. Tarascon, C. Masquelier, Nat. Mater. 4 (2005) 254.
[2] P. Subramanya Herle, B. Ellis, N. Coombs, L.F. Nazar, Nat. Mater. 3 (2004) 147.
[3] S.-Y. Chung, J.T. Bloking, Y.-M. Chiang, Nat. Mater. 1 (2002) 123.
[4] A.K. Padhi, K.S. Nanjundaswamy, J.B. Goodenough, J. Electrochem. Soc. 144 (1997) 1188.
[5] A. Ait Salah, P. Jozwiak, J. Garbarczyk, K. Benkhouja, K. Zaghib, F. Gendron, C.M. Julien, J. Power Sources 140 (2005) 370.
[6] S. Patoux, C. Wurm, M. Morcrette, G. Rousse, C. Masquelier, J. Powder Sources 119–121 (2003) 278.
[7] C. Masquelier, A.K. Padhi, K.S. Nanjundaswamy, J.B. Goodenough, J. Solid State Chem. 135 (1998) 228.
[8] M. Sato, S. Yajimi, H. Okawa, K. Uematsu, K. Toda, Solid State Ion. 152–153 (2002) 247.
[9] A.K. Ivanov-Schitz, A.V. Nistuk, N.G. Chaban, Solid State Ion. 139 (1–2) (2001) 153.
[10] P. Eyob, A.S. Andersson, J.O. Thomas, J. Mater. Chem. 12 (8) (2002) 2343.
[11] M. Morcrette, C. Wurm, C. Masquelier, Solid State Sci. 4 (2002) 239.
[12] G. Rousse, J. Rodríguez-Carvajal, C. Wurm, C. Masquelier, Appl. Phys. A: Mater. Sci. Proccess. 74 (2002) S704.
[13] G. Rousse, J. Rodríguez-Carvajal, C. Wurm, C. Masquelier, Chem. Mater. 13 (12) (2001) 4527.
[14] C. Masquelier, C. Wurrn, J. Rodríguez-Carvajal, J. Gaubicher, L. Nazar, Chem. Mater. 12 (2000) 525.
[15] A.S. Andersson, B. Kalska, P. Jonsson, L. Haggstrorn, P. Nordblad, R. Tellgren, J.O. Thornas, J. Mater. Chem. 10 (2000) 2542.
[16] J.L. Zarestky, D. Vaknin, B.C. Chakoumakos, T. Rojo, A. Goñi, G.E. Barberis, J. Magn. Magn. Mater. 134 (2001) 401.
[17] J.L. Mesa, A. Goñi, A.L. Brandl, N.O. Moreno, G.E. Barberis, T. Rojo, J. Mater. Chem. 10 (2000) 2779.
[18] N.O. Moreno, J.L. Mesa, A. Goñi, A.L. Brandl, T. Rojo, G.E. Barberis, J. Magn. Magn. Mater. 226-230 (2001) 1073.
[19] A.B. Bykov, A.P. Chirkin, L.N. Dernyanets, S.N. Doronin, E.A. Genkina, A.K. Ivanov-Shits, L.P. Kondratyuk, B.A. Maksirnov, O.K. Mel'nikov, L.N. Muradyan, V.L. Sirnonov, V.A. Timofeeva, Solid State Ion. 38 (1990) 31.
[20] A. Goñi, L. Lezama, N.O. Moreno, L. Fournes, R. Olazcuaga, G.E. Barberis, T. Rojo, Chem. Mater. 12 (2000) 62.
[21] J. Rodríguez-Carvajal, Physica B 192 (1993) 55.
[22] E.F. Bertaut, J. Phys. 32 (1971) C1.
[23] L. Rossat-Mignot, Magnetic Structures and Neutron Diffraction, Academic Press, New York, 1987.
[24] (a) G.L. Long, G. Longworth, P. Battle, A.K. Cheetham, R.V. Thundathil, D. Beveridge, Inorg. Chem. 18 (1979) 624;
(b) P.D. Battle, A.K. Cheeetham, G.J. Long, G. Longworth, Inorg. Chem. 21 (1982) 4223;
(c) P.D. Battle, A.K. Cheethem, W.T.A. Harrison, G.J. Long, J. Solid State Chem. 62 (1986) 16;
(d) L. Néel, Ann. Phys. (Paris) 3 (1948) 137;
(e) T. Moya-Pizarro, R. Salmon, L. Fournes, G. LeFlem, B. Wanklyn, P. Hagenmuller, J. Solid State Chem. 53 (1984) 387.